Understanding Dissipative Tip–Molecule Interactions with Submolecular Resolution on an Organic Adsorbate

Gernot Langewisch, Wojciech Kamiński, Daniel-Alexander Braun, Rolf Möller, Harald Fuchs, André Schirmeisen,* and Rubén Pérez**

Three-dimensional force spectroscopy measurements on 3,4,9,10-perylene-tetracarboxylic dianhydride adsorbed on Ag(111) are combined with first-principles calculations to characterize the dissipative tip–molecule interactions with submolecular resolution. The experiments reveal systematic differences between the energy dissipation at the end groups and the center of the molecules that change with the tip–sample distance. Guided by the strength of the experimental conservative forces, an Ag-contaminated Si tip is identified as the likely tip termination in the experiments. Based on this tip configuration, the energy dissipation in the tip–sample contact is determined from the approach and retraction force curves calculated as a function of distance for different molecule sites. These calculations provide an explanation for the experimental trends in terms of the competition between localized dissipation mechanisms involving the quite mobile oxygen atoms on the sides of the molecule, and global molecular deformations involving the more rigid perylene core. The results confirm that the observed dissipation can be explained in terms of adhesion hysteresis and show the power of combined experimental–theoretical spectroscopy studies in the characterization of the underlying microscopic mechanisms.

1. Introduction

For structural investigations of surfaces down to the atomic scale, noncontact atomic force microscopy (nc-AFM) is a proven technique.[1] In contrast to the often deployed scanning tunneling microscopy (STM), it is not limited to conducting surfaces. Besides high-resolution surface scans, force interactions between the tip and the sample can be measured

---

G. Langewisch, Dr. D.-A. Braun,[+] Prof. H. Fuchs
Physikalisches Institut
Universität Münster
Wilhelm-Klemm-Str. 10, 48149 Münster, Germany
and Center for NanoTechnology (CeNTech)
Heisenbergstraße 11, 48149 Münster, Germany
E-mail: g.langewisch@uni-muenster.de

Dr. W. Kamiński
Institute of Experimental Physics
University of Wrocław
plac Maksa Borna 9, 50-204 Wrocław, Poland

Dr. W. Kamiński, Prof. R. Pérez
Departamento de Física Teórica de la Materia Condensada
Universidad Autónoma de Madrid
28049 Madrid, Spain
E-mail: ruben.perez@uam.es

Prof. R. Möller
Center for Nanointegration Duisburg-Essen
Universität Duisburg-Essen
Lotharstraße1–21, 47057 Duisburg, Germany

Prof. A. Schirmeisen
Institut für Angewandte Physik
Universität Gießen
Heinrich-Buff-Ring 16, 35392 Gießen, Germany
E-mail: Andre.Schirmeisen@ap.physik.uni-giessen.de

[+] Current address: Heidelberg Instruments Mikrotechnik GmbH,
Tullastraße 2, 69126 Heidelberg, Germany

DOI: 10.1002/smll.201101919

quantitatively by nc-AFM. For instance, by site-specific force spectroscopy, atomic-scale information about surface chemical reactivity and binding forces was obtained.[2] This method was recently extended to 3D force-field spectroscopy, in which spectroscopy curves are recorded along a grid parallel to the sample surface providing three-dimensional landscapes of interaction forces and potentials.[3,4]

Over the past two decades, there has been an increasing interest in organic thin films motivated by potential applications in organic semiconductor devices. In these devices, the structure of organic assemblies on the nanometer scale, for instance the molecular packing, plays an important role due to its effect on the electronic or optoelectronic characteristics of the functional organic layers.[5] In this respect, nc-AFM can provide valuable information about structural properties. Although high-resolution imaging of organic molecules still remains a challenging task due to the complex interplay of long- and short-range tip–sample interactions, submolecular and even atomic resolution was achieved in recent years.[6–8] Furthermore, 3D force-field spectroscopy was successfully applied to identify the tip–sample interactions leading to atomic resolution on organic molecules.[8]

In addition to conservative tip–sample forces, dissipative interactions can be studied by nc-AFM.[9] Two different signals are simultaneously recorded in nc-AFM: the frequency shift that renders the topography, and the so-called dissipation (or damping) signal which is a measure of the additional amount of energy required to keep the oscillation amplitude constant, compensating for the energy lost in the cantilever due to the nonconservative tip–sample interactions.[10,11] The dissipation images also show true atomic resolution and thus provide a tool to study dissipation at the atomic scale on semiconductor, ionic, and carbon surfaces.[9,12,13]

While a general consensus exists in the interpretation of the nc-AFM topography images, the connection between the dissipation images and some physical energy-dissipation processes is still very controversial.[9,14–23] Some authors consider van der Waals friction or stochastic friction to be the origin of dissipation while other theoretical models are based on adhesion hysteresis effects.[24–27] Recently, a combination of theory and dynamic AFM experiments on semiconductor surfaces and adsorbed sexithiophene layers has provided strong support for adhesion hysteresis as the dominant mechanism of energy dissipation in the near-contact regime.[13,28,29] These studies show that the measured energy dissipation per oscillation cycle can be quantitatively explained by the hysteretic behavior of the tip–sample force versus distance curves. The force hysteresis is associated with the complex configuration space of the tip–sample system, with multiple local energy minima separated by energy barriers. These barriers break the adiabaticity, as the system is trapped in different local energy minima during approach and retraction of the AFM tip, and lead to force hysteresis and energy dissipation.

Herein, we face the challenge of extending the characterization of the dissipative interactions to organic adsorbates by combining 3D force-field experiments that achieve submolecular resolution with first-principles calculations. The system that we have considered, the organic semiconductor 3,4,9,10-perylenetetracarboxylic dianhydride (PTCDA) adsorbed on the Ag(111) surface, is the paradigmatic example of an organic/inorganic interface. PTCDA adsorbed on noble metal surfaces has been extensively studied experimentally and theoretically to understand the mechanisms controlling the band alignment at the interface.[30–37] The well-characterized system formed by a single monolayer of PTCDA deposited on the Ag(111) surface is therefore an ideal model system to explore the intramolecular dissipation contrast that we observed with nc-AFM and to investigate the atomic-scale mechanisms involved in the dissipation of energy. From the 3D force-field measurements, we extracted force and dissipation spectroscopy curves that can be assigned to different parts of the molecules. These curves show systematic differences between the end groups and the center of the molecules that change with the tip–sample distance. Using first-principles methods, force versus distance curves on different molecule sites for the approach and retraction of three tip models are calculated. By comparing the experimental interaction strength with the theoretical average forces, we determine the likely tip termination in our experiments as an Ag-contaminated Si tip. The energy dissipation associated with the variation in the approach and retraction force curves for this tip on the different sites and for different closest-approach distances provides an explanation for the experimental trends. These calculations confirm adhesion hysteresis as the dominant dissipation mechanism in the near-contact regime and help to identify the atomic-scale mechanisms involved.

2. Experimental Details

2.1. Experimental Setup and Sample Preparation

The measurements were performed at room temperature with an ultrahigh-vacuum atomic force microscope (Omicron VT-AFM) in the frequency modulation (FM) mode utilizing an additional frequency demodulator (Nanonis PLL).[38] A silicon cantilever with integrated tip was used as a force probe (Nanosensors NCHR-SSS type, resonance frequency f_0 = 298 kHz, spring constant k = 27 N m^{-1}, oscillating with an amplitude of A = 8 nm. The oscillation was detected by the laser beam deflection method. To remove the contaminations prior to the experiment, the tip was sputtered with Ar ions. The metal single crystal, Ag(111) (Mateck GmbH, Germany), which was used as substrate for the PTCDA molecules, was prepared by repeated cycles of Ar-ion sputtering and annealing at a temperature of approximately 650 K. The PTCDA (Sigma–Aldrich) was evaporated from a quartz crucible at about 470 K for 45 s resulting in a submonolayer coverage.

2.2. Experimental Method: Force and Dissipation Spectroscopy

Conservative force interactions between the AFM tip and the sample surface can be measured quantitatively by force spectroscopy. For this, the frequency shift of the cantilever oscillation is recorded as a function of relative tip–sample distance. These frequency shift curves can then be converted

DOI: 10.1002/smll.201101919

into tip–sample forces. However, the lateral accuracy of single-point force spectroscopy is usually not sufficient to investigate site-specific forces on the atomic or submolecular scale, especially at room temperature. A more precise way to study such interactions with high spatial resolution is 3D force-field spectroscopy.[3,4] Here, many equidistant spectroscopy curves are recorded along a grid across the sample. These curves can then be assembled to a three-dimensional landscape of tip–sample force or interaction potential, which allows correlation of features in this landscape to different atomic sites.[3,20,23,39] In addition, a topography scan at a constant detuning Δf is typically recorded together with the force-field measurements. Each time one of the predefined grid positions is reached, this scan is interrupted for the acquisition of the corresponding spectroscopy curve. The surface topography provides an additional reference to assign spectroscopy measurements to certain positions on the sample surface.

For our force-field measurements, we defined a grid of 50 points along the x direction and five points along the y direction covering a surface area of 3.5×3.5 nm^2. Here, the x direction is defined as the fast scanning direction and the y direction is the slow scanning direction of the simultaneously recorded topography scan. The relatively high lateral point density in the spectroscopy slices along the x direction allowed us to study tip–sample interactions with submolecular resolution. However, the thermal drift during the acquisition time of about 1.8 min per slice was around 0.1 nm, which limited the reasonable number of grid points in the y direction considerably.

The focus of these investigations was, however, to study the nonconservative interactions leading to energy dissipation in the tip–sample contact. This physical quantity can also be determined by nc-AFM. In the spectroscopy experiments, we recorded the amplitude of the excitation signal V_{exc} for the cantilever oscillation simultaneously with the frequency shift Δf. As the AFM instrument is operated in constant amplitude mode, the excitation amplitude is adjusted by the feedback loop to maintain the cantilever oscillation constant and is therefore a measure of the energy dissipated during one oscillation cycle. Assuming that the frequency shift of the oscillation caused by the tip–sample forces is small compared to the resonance frequency of the cantilever, a quantitative relation between the energy loss per oscillation cycle ΔE and the experimental parameters is given by:

$$\Delta E = \pi \frac{c_z A^2}{Q} \left(\frac{V_{\text{exc}}}{V_{\text{exc},0}} - 1 \right) \tag{1}$$

where c_z is the spring constant, A the oscillation amplitude, Q the effective quality factor, and $V_{\text{exc},0}$ the excitation voltage for a free oscillating cantilever.[40,41]

3. Theoretical AFM simulations: Model and Computational Details

3.1. Simulation Method: Fireball

We performed first-principles calculations based on density functional theory (DFT) with a local-orbital basis using the Fireball code.[42] This code is designed to deal with large-scale simulations and offers a very favorable accuracy-to-efficiency balance provided that the basis set is carefully chosen.[43] Given the size of the system we want to simulate, and the need to calculate a large set of force versus distance curves with the different tip models that we consider, this fast approach is the method of choice. In Fireball, as in most of the DFT codes using a local basis, the wave functions of valence electrons are expanded in terms of the so-called Fireball orbitals, that is, a set of strictly localized pseudo-atomic orbitals, which are exactly zero for distances larger than the cutoff radius R_C.[44] We used the following optimized basis set of numerical atomic orbitals: *s* for H, *sp* for C, O, and Si, and *spd* for Ag.[28,29,43] The cutoff radii (in a.u.) of those orbitals are: 4.1 (*s*) for H, and (4.5, 4.5), (3.3, 3.8), (4.8, 5.4), and (5.3, 5.7, 4.5) for orbitals of C, O, Si, and Ag, respectively. The results obtained with this basis set for the relevant structural and electronic properties of the PTCDA molecule, the Ag(111) surface, and the AFM tips that we considered (see below) are an excellent match with fully converged plane-wave DFT calculations (using VASP).[45]

The calculations presented herein are performed within the local density approximation (LDA) for the exchange-correlation functional.[46] Although the proper theoretical description of systems where van der Waals (vdW) interactions play a significant contribution to the bonding is still under discussion, LDA provides a realistic description of the molecule–substrate bonding distances and the interface electronic properties, in agreement with studies combining gradient-corrected functionals (like PBE) and a semiempirical force field or a fully nonlocal vdW functional to describe the vdW interactions.[37,47,48] The same considerations apply to the inclusion of the vdW contributions in the tip–sample interaction. The known overbinding associated with the DFT-LDA approach effectively includes, together with the short-range chemical interaction, the microscopic vdW contribution due to the closest atoms in the tip and sample. Long-range vdW interactions associated with the macroscopic parts of tip and sample, not contributing to the atomic-scale spatial contrast, are not included in the calculations.

3.2. Modeling the PTCDA/Ag Interface

The adsorption of 1 monolayer of PTCDA on Ag(111) has already been characterized by experiment and theory.[48,49] The unit cell we have used, containing two PTCDA molecules forming a herringbone pattern (see **Figure 1**), is a nearly rectangular (6,1,–3,5) superstructure of the Ag(111) surface, with lattice vectors of 18.92 and 12.58 Å, which correspond to our theoretical lattice constant of 4.08 Å for bulk Ag.[48] The Ag substrate is modeled with a three-layer slab (each Ag monolayer contains 33 atoms). Tests with a six-layer slab show no significant difference. The unit cell (the Ag slab and the two PTCDA molecules) contains 175 atoms. Only the Γ point has been included in the sampling of the Brillouin zone. In our relaxed, ground-state configuration, the adsorption sites of the two molecules are not equivalent (see Figure 1): one molecule (A) is nearly perfectly aligned

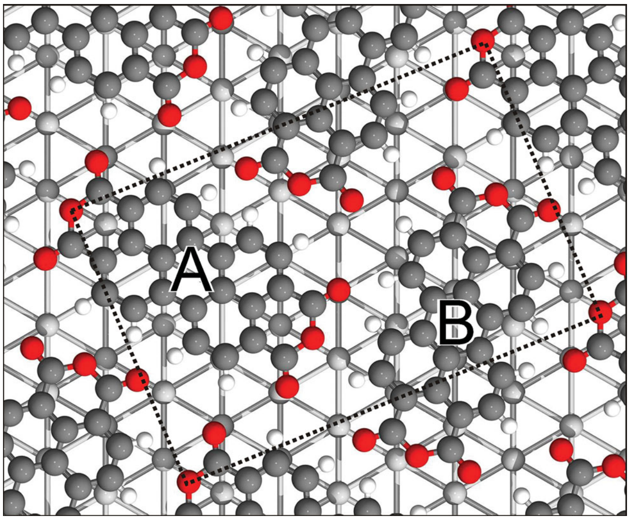

Figure 1. Top view of the herringbone structure of the PTCDA monolayer adsorbed on the Ag(111) surface. The unit cell is marked by the dotted black line and the molecules A and B are denoted as well. Color code for the atoms: oxygen (red), silver (light gray), carbon (dark gray), and hydrogen (white).

with the Ag(111) lattice while the other molecule (B) is misaligned by 17°, in agreement with previous theoretical calculations.[48] Our DFT-LDA approximation provides a bonding distance of 2.83 Å (X-ray standing wave (XSW) experiment gives 2.86 Å), and a very good description of the projected density of states around the Fermi level (not shown) found in both scanning tunneling spectroscopy (STS) and ultraviolet photoelectron spectroscopy (UPS) experiments, thereby confirming the validity of the DFT-LDA approximation for the description of such organic/metal interfaces.[30,49,50]

3.3. AFM Tip Models and Simulations

The identification of the tip-apex termination, which controls the tip–sample forces, is a crucial step in the understanding of the experimental results. In the absence of direct information from the experiment, our standard procedure is to look for tips that reproduce the forces measured in the experiment. As Si cantilevers are used in the experiments, we considered three models that covered clean and contaminated Si tips (see **Figure 2**): a) an H3-(111)-oriented Si tip (10 Si atoms + 15 hydrogen atoms saturating the tip base) used in our previous studies, b) a Si oxide tip constructed from a very stable SiO_2 cluster (containing 39 atoms), and c) an Ag-contaminated Si tip (Ag-Si), where the Si atom at the apex of the H3-Si tip is replaced by an Ag atom.[28,29,51,52] These tips have a different electronic character, and expand a wide range of chemical reactivities and interaction strengths as discussed below.

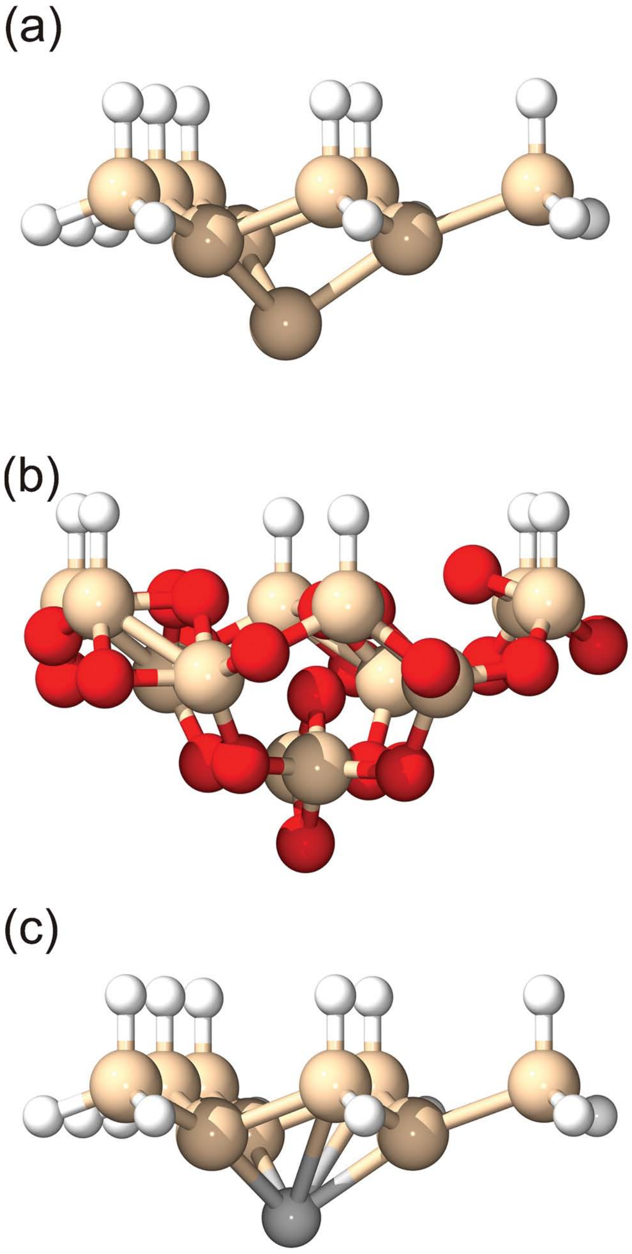

Figure 2. Models of the AFM tip considered in simulations: a) an H3-(111)-oriented Si tip (10 Si and 15 H atoms saturating the tip base), b) a Si oxide tip (39 atoms in total), and c) an Ag-contaminated Si tip (Ag-Si), where the Si atom at the apex of the H3-Si tip is replaced by an Ag atom. Color code for the atoms: silicon (light salmon), hydrogen (white), silver (light gray), and oxygen (red).

For all these tips, we determined tip–sample forces during approach and retraction for different sites over the PTCDA/Ag(111) unit cell (the specific sites and the range of tip–sample distances covered are discussed in Section 5). We used a quasi-static approach, at temperature $T = 0$, by approaching/retracting the tip along the normal to the surface in steps of 0.25 Å. At each approach/retraction step all of the atoms in both the PTCDA/Ag sample and the AFM tip (except for the bottom layer of the slab and top layer of the tip) were allowed to relax to their ground-state configuration using both a conjugate gradient minimization and a dynamical quenching method, with the following convergence criteria: 10^{-4} eV atom^{-1} for changes in the total energy and 0.1 eV Å^{-1} for maximum force acting on the free atoms. The total short-range tip–sample forces were then calculated as a sum of the

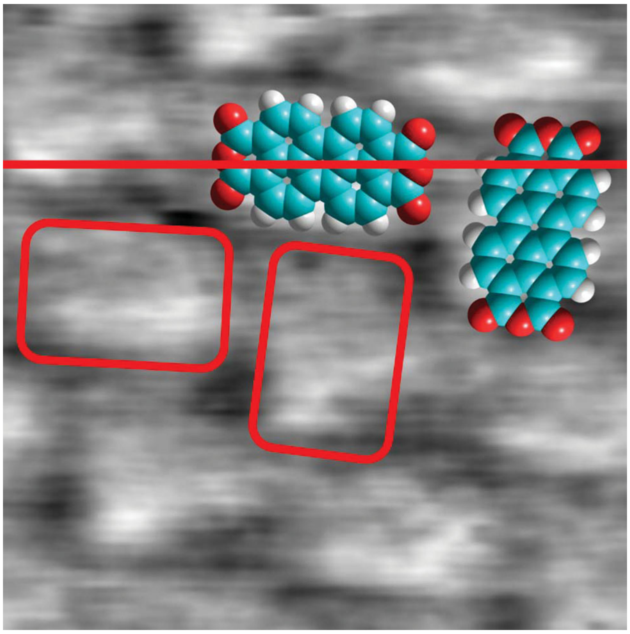

Figure 3. Topography scan (3.5 × 3.5 nm^2) of PTCDA adsorbed on Ag(111). Sketches of PTCDA molecules indicate the position of individual molecules. The solid red line marks exemplarily a path along which a frequency shift slice was obtained.

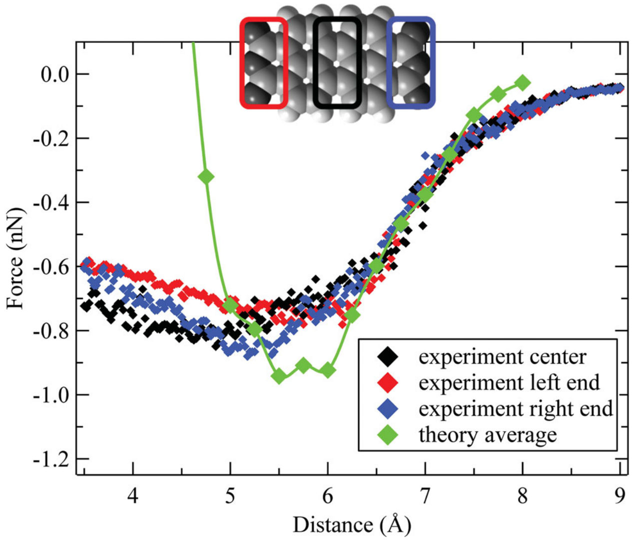

Figure 4. Experimental and calculated force versus distance curves. In the experiment, only those molecules that were in line with the *x* direction were investigated and the results of several measurements on different molecules were averaged. Tip–molecule forces at the center of the molecules are represented by black, at the left end group by red, and at the right end group by blue markers. The corresponding molecule sites are indicated in the sketch (inset). The DFT calculations were performed with an Ag-Si tip that probes the 4–8 Å tip–sample distance range, and the resulting force curves were averaged over approach and retraction for all the 14 tip positions considered over the two different molecules A and B of the unit cell. The tip–sample distance is measured with respect to the last Ag layer. PTCDA molecules are about 2.8 Å above the Ag surface.

final forces acting on the tip atoms, which were kept fixed during the relaxation process at each tip–sample distance.

4. Results of Force and Dissipation Spectroscopy

Figure 3 shows a 3.5 × 3.5 nm^2 topography scan of a PTCDA layer adsorbed on the Ag(111) surface. This scan was recorded at a constant frequency shift of $\Delta f = -60$ Hz. During the scan as well as during the spectroscopy measurements, a bias voltage of 0.5 V was applied to the tip to compensate electrostatic forces. Based on the method described by Dürig, the frequency shift in the spectroscopy curves was converted into tip–sample forces while the dissipated energy was calculated from the excitation voltage according to Equation (1).[53] Sketches of PTCDA molecules indicate the position of individual molecules, which are arranged in the typical herringbone pattern. The fast scan direction is aligned parallel to one of the two different molecular orientations. The position of one of the five slices of a spectroscopy grid is illustrated exemplarily by a red line (see Figure 3). Based on the topography scans which were recorded together with the force-field spectroscopy measurements, the spectroscopy curves of the slices could be assigned to different parts of the molecules. We limited the analysis to those molecules whose long axis was parallel to the *x* direction, as only for these molecules was the lateral point density of the spectroscopy grid high enough to allow a precise assignment. For the analysis of site-specific effects, we distinguished between the left and the right end group (relative to the orientation in the topography scan) and the center of the molecules. For each of these molecule sites, six spectroscopy curves obtained on different molecules (extracted from two consecutive force-field measurements) were averaged. Due to the fact that the molecule structure could not be imaged with atomic resolution, a clear assignment of the spectroscopy curves to the different oxygen atoms at the end groups was not possible. To account for site-specific distinctions in the tip–sample interactions, we averaged curves equally distributed within larger areas covering the estimated positions of the central carbon ring at the center and the oxygen atoms at the end groups of the molecules (see sketch in **Figure 4**). In addition, the averaging of several spectroscopy curves is an effective procedure to minimize experimental noise.[54,55] Consequently, the noise in the individual spectroscopy curves, which was about 0.2 nN in the force and about 0.05 eV per oscillation cycle in the dissipation before averaging, was significantly reduced (note that no additional smoothing was applied).

In Figure 4, the tip–sample forces obtained in the experiment for the different molecule sites are shown. Included in the figure are also the corresponding results of the DFT calculations. This theoretical curve is an average of the force curves calculated for approach and retraction for all the 14 tip positions considered over the two different molecules A and B of the unit cell, as discussed in Section 5. Due to the fact that only relative tip–sample distances are known in the experiment, the zero point of the experimental distance axis had to be adjusted to allow a comparison with the theory. Here, the force curves provide a proper reference for the alignment. In this context, one has to take into account that certain interactions and processes that are present in the experiment could not be considered in the calculation. First, attractive long-range vdW forces are not included in the simulations. In the experiment, they dominate the interactions at large tip–sample distances before the onset of site-specific attractive short-range forces (note that long-range electrostatic forces are compensated by the tip bias), while at small distances they partly compensate repulsive short-range interactions. Second, due to the small size of the nanoasperity modeling the tip, the simulations cannot describe correctly the elastic deformation of the tip (see Section 5) which can be assumed at small distances beyond the minimum of the force curves with the onset of repulsive interactions. Consequently, the criterion for the adjustment of the distance axis was a maximal agreement between theoretical and experimental force curves in the regime of short-range attractive interactions before the force minimum. To estimate the starting point of this regime in the spectroscopy measurements, we compared the force curves obtained on different molecule sites. At large distances, the curves are virtually identical. This is the regime which is dominated by vdW interactions. With decreasing distance, starting at about 7.5 Å, variations between the curves appear, which can be attributed to short-range interactions as they typically show site-specific characteristics. Thus, the regime that is optimal for the adjustment of the distance axis is between this point and the minimum of the force curves. While the variations are barely visible in Figure 4 within the experimental noise in the distance range between 7.5 and 6.5 Å (one has to subtract the curves from each other to emphasize the differences), they become more obvious at smaller distances. In particular, the force minima (the points of maximum attractive interaction) at the end groups are shifted towards larger distances in relation to the center of the molecule. However, the forces at the minima differ only slightly and are about 0.8 nN.

The dissipation spectroscopy curves, which were recorded together with the force curves in Figure 4, are shown in **Figure 5**. The energy dissipation starts at a distance of about 7.5 Å approximately coinciding with the onset of short-range interactions, and increases monotonously upon approach of the tip. At the point of closest approach, it reaches values up to 0.8 eV per oscillation cycle. The dissipation differs for the different molecule sites, showing an asymmetry between left and right ends. Nevertheless, when comparing the curves, a systematic common trend at the end groups in comparison to the center can be observed. In the distance range between 6 and 5 Å, the dissipation at the end groups is higher whereas the opposite is the case at distances below 4.5 Å.

For a direct comparison with the experiment where only one of the two molecules of the unit cell was investigated, the corresponding results of the simulations for both molecules (upper part: molecule A, lower part: molecule B) are included in Figure 5. Here, the energy dissipation was calculated from the hysteresis in the simulated force curves during approach and retraction to three distances of closest approach of 3.2, 2.2, and 1.2 Å above the PTCDA molecules. This corresponds to distances of 6, 5, and 4 Å above the Ag surface, which is the reference for the distance scale in the figures. Please note that the dotted lines connecting the theoretical data points are only guides to the eye. At distances of 6 and 5 Å, no significant differences between the two molecules can be observed whereas at the distance of 4 Å, characteristic distinctions between molecules A and B are found in the simulations resulting in differences in the dissipation at the molecule end groups in relation to the center.

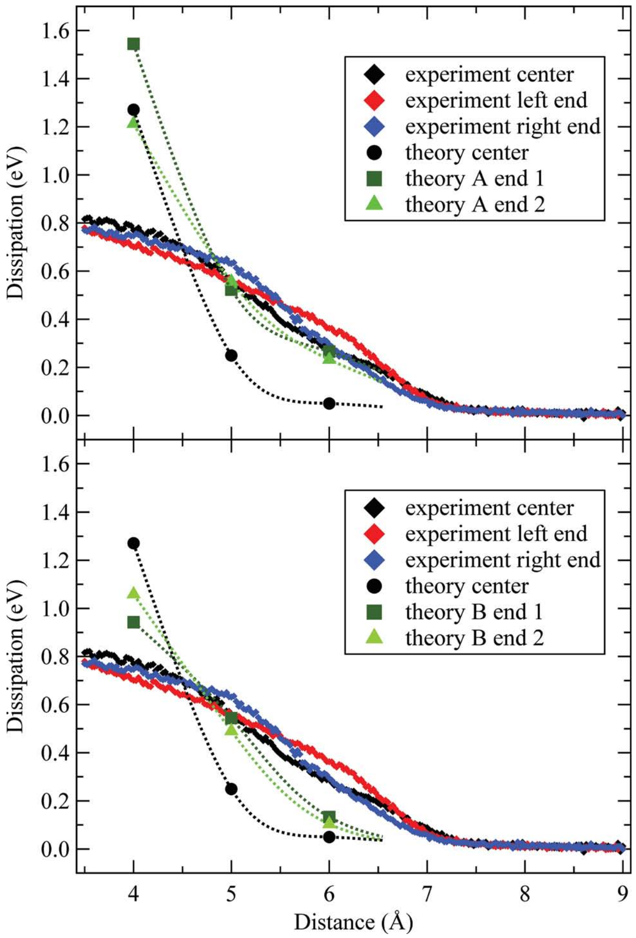

Figure 5. Comparison of the energy dissipation per oscillation cycle at different molecule sites measured in the experiment with the corresponding calculations for molecules A (top) and B (bottom). The dissipation spectroscopy curves for the center (black), the left end group (red), and the right end group (blue) of the molecules that were in line with the *x* direction are shown. The results of the simulations are represented by black (center of the molecule), dark green (end group 1), and light green (end group 2) markers. The dissipation was calculated from the forces during approach and retraction to three distances of closest approach of ≈3.2, 2.2, and 1.2 Å above the PTCDA molecules (see Figure 7), which correspond to the attractive, near-contact, and repulsive regimes in the interaction. The dotted lines are guides for the eye.

For a detailed analysis of the energy dissipation at the different molecule sites, we subtracted the results of the dissipation at the center from the values at the ends. The resulting experimental curves are illustrated in **Figure 6** (top). The general behavior of the dissipation at the ends in relation to the center is qualitatively and quantitatively very similar for left and right sides. The only substantial deviation between the sides arises in the distance regime between 7.5 and 6.2 Å

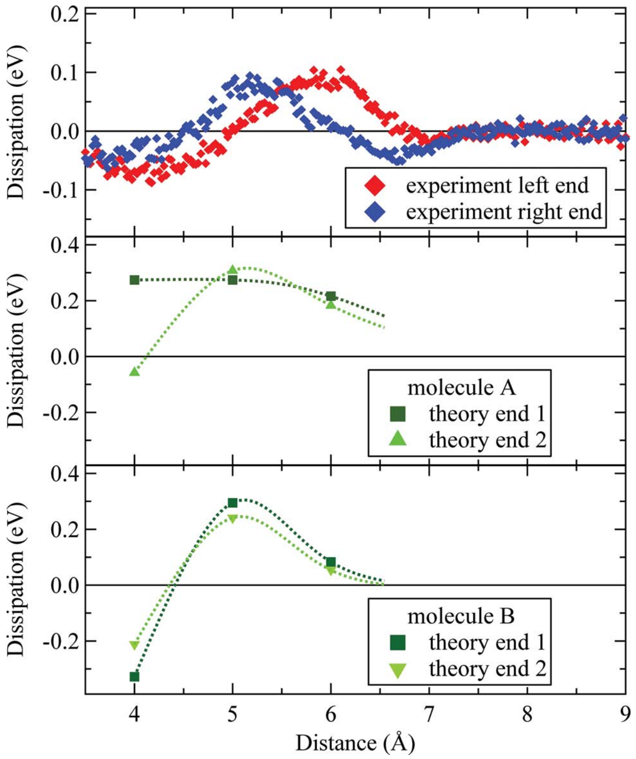

Figure 6. Site-specific differences of the dissipation; top: experiment, center: theory molecule A, bottom: theory molecule B. The energy dissipation per oscillation cycle at the center is subtracted from the values at the end groups. Note that the vertical axes are scaled with different factors for better clarity. The experimental curves (left end: red line, right end: blue line) are compared with the theoretical results (end 1: dark green squares, end 2: light green triangles) for three indentation depths, 2, 3, and 4 Å, which correspond to distances of closest approach of ≈3.2, 2.2, and 1.2 Å above the PTCDA molecules. The dotted lines are only guides for the eye.

after the onset of dissipative interactions. Here, the values at the sides are smaller than at the center. At the right end, this regime extends over 1.3 Å while at the left end, it is only half as broad. This leads to a shift of about 0.6 Å between the two curves, which are otherwise almost identical. When further decreasing the distance, the dissipation at the ends starts to dominate and is up to ≈0.1 eV higher at both ends than at the center. This regime extends over 1.6 Å up to the point where this relation is reversed and the difference in dissipation becomes negative again for the rest of the investigated distance range.

An aspect that has to be considered is the possible influence of an asymmetric tip structure on the interactions between the tip and the two opposite end groups of the molecules. The shift between the spectroscopy curves at the left and the right end groups could indeed be the effect of a minor asymmetry of the tip in the *x* direction. However, besides this shift, the site-specific behavior of both ends in relation to the center of the molecules is very similar. Thus, we believe that the effect of an asymmetry in the *x* direction does not play a crucial role. A possible asymmetry of the tip in the *y* direction is not relevant for a comparison of tip–sample interactions at different molecule sites along the *x* axis.

The middle and lower part of Figure 6 shows the differences in the dissipation between end groups and the center of the molecules found in the simulations (center: molecule A, bottom: molecule B). At distances of 6 and 5 Å, the dissipation at the end groups is up to ≈0.3 eV higher with no significant deviations between molecules A and B. However, as discussed before, such differences can be observed at a distance of 4 Å. For molecule A, the dissipation at one end is about 0.3 eV higher and at the other end slightly lower than at the center. In the case of molecule B, lower dissipation was found for both ends—with a difference of up to ≈0.3 eV compared to the center—which nicely reproduces the trend found in the experimental results: higher dissipation at the ends at a distance of 6 and 5 Å, lower dissipation at 4 Å.

5. Understanding the Contrast: Theory versus Experiment

In this section, we compare the experimental results discussed so far with calculations for the tip–sample interaction and the energy dissipated per oscillation cycle. In the case of the forces, the procedure is quite straightforward—the comparison between the experimental and theoretical results would allow us to identify a likely termination for the experimental tip apex. As experiments do not achieve atomic resolution inside the molecule, we do not attempt a detailed characterization of the tip apex as it has been achieved in semiconductor surfaces.[13] We rather confine ourselves to determine, using the large differences in the strength of the interaction averaged over different sites, a family of tips that could provide a reasonable explanation of the observed contrast, in this case a metal-contaminated Si tip (see Figure 2c). Based on this Ag-Si tip, we explore the possibility to explain the experimental contrast provided by the energy dissipation. Our calculations support adhesion hysteresis as the relevant short-range dissipation mechanism and provide an explanation for the trends in the variation of dissipation with the tip–sample distance found in the experiment.

5.1. Characterizing the AFM Tip Termination: Experimental versus Theoretical Site-Averaged Forces

To gain insight into the strength of the interaction, the induced sample deformations, and possible atomistic mechanisms for energy dissipation, we performed force versus distance calculations for each of the three tips (see Figure 2) on 14 different positions of the unit cell: 12 positions correspond to sites on top of each O atom in the two PTCDA molecules and the other two positions are associated with a carbon atom on the center of the perylene core of molecules A and B, respectively. For all of these positions of the AFM tip over the PTCDA/Ag sample, we started the approach at a position where the last tip atom is at a distance 8 Å above the last Ag layer that is taken as the distance reference. This position corresponds to a distance of ≈5.2 Å above the perylene core of the PTCDA molecules. From this point, where the interaction is negligible, three approach/retraction cycles were simulated where the tip–sample distance is reduced in steps of 0.25 Å, a total of 2, 3, and 4 Å (we refer, for simplicity, to these values as the indentation depth), and then retracted back to the original position, while calculating the forces during the process. The final approach distances of ≈3.2, 2.2, and 1.2 Å correspond to the attractive, near-contact, and repulsive regimes in the interaction.

Our force calculations with the three tips do show differences between the sites that should result in atomic-scale image contrast inside the molecules. As only small differences between different molecule sites can be observed in the experiment, we decided to average our force curves over all the calculated sites to compare the interaction strength. Our results for the clean Si tip clearly indicate a very strong interaction with the PTCDA molecules. Attractive tip–sample forces as large as ≈3 nN are found during tip retraction. These forces are large enough to lift the molecule from the surface. On the contrary, force versus distance curves for the Si oxide tip present very small attractive forces and no significant deformation of the PTCDA/Ag sample until the contact regime where repulsive forces dominate. This behavior translates into very small force hysteresis, and thus negligible energy dissipation values. The Ag-contaminated Si tip has an intermediate behavior between the two extreme cases. The maximum attractive force of ≈0.95 nN compares well with the experimental results (approximately 0.80 nN, see Figure 4). Force spectroscopy experiments are sensitive to the conservative part of the tip–sample interaction. The average of the approach and retraction forces gives access to this conservative interaction, while the difference is responsible for the energy dissipation. Thus, to compare with the experiments, the green curve in Figure 4 represents the average of the force versus distance curves for approach and retraction, for the indentation depth of 4 Å, for all 14 positions calculated with the Ag-Si tip. According to the absolute distance scale that we can set in the calculations, the position of the force maximum would correspond to a distance of ≈2.2 Å between the tip apex and the PTCDA molecules.

While short-range attractive forces are well reproduced with the Ag-Si tip, the repulsive part markedly differs from the experimental data. This discrepancy is possibly caused by the artificially large hardness of our small tip model, where the atoms in the top layer are fixed and only the last four atoms in the apex are allowed to relax. This small nanoasperity cannot capture the elastic response of the real tip apex and consequently, forces in the repulsive regime are overestimated.

5.2. Energy Dissipation with the Ag-Si Tip

Our calculations with the Ag-Si tip reveal a significant hysteresis in the approach/retraction force curves. **Figure 7** shows the tip–sample force versus distance curves, averaged on the tip positions associated with the center (carbon atoms) and ends (oxygen atoms) of the two molecules in the unit cell, for two of the three distances of closest approach that we have considered. In all the cases we started at a tip–sample distance where there is no significant interaction (8 Å from the last Ag layer, ≈5.2 Å above the PTCDA molecules) and approached the tip by 2, 3, and 4 Å.

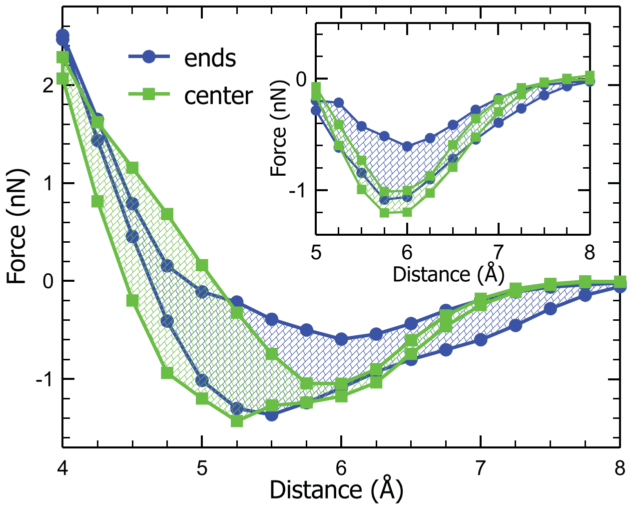

Figure 7. Force versus distance curves for the approach/retraction of the Ag-Si tip for two different indentation depths: 3 Å (see inset) and 4 Å, averaged over all O tip positions (blue) and on the center of perylene cores (green). The distance scale is with reference to the outermost layer of the Ag surface.

For a total distance approach up to 3 Å, like the one illustrated in the inset of Figure 7, the energy dissipation at the ends of the PTCDA molecules (blue) is larger than at the perylene cores (green). The Ag-Si tip induces “flipping” of the more mobile O atoms, which leads to an enhanced dissipation signal at the ends of the molecules. In particular, **Figure 8**a illustrates that “bonds” between the PTCDA molecule and both the Ag-Si tip and one of the Ag surface atoms are formed when the Ag-Si tip—located on the top of the anhydride oxygen atom—approaches the PTCDA/Ag sample. This tip–sample geometry reveals a deformation of the end of the molecule which differs from the configuration at the same tip–sample distance (5.25 Å) during retraction of the tip. In this case, a Ag atom on the apex of the tip is bonded to the carbon atom of the molecule (see Figure 8b). The presence of these two local energy minima, where the system is trapped during approach and retraction, gives rise to the energy dissipation.

Our calculations reproduce clearly the trend found in the experiments: at closer distances, the dissipation at the center of the molecules becomes larger than on the sides. The force curves in Figure 7 for a total distance approach of 4 Å show a larger force hysteresis on the carbon atoms in the perylene core (green area). Figure 8d and e illustrate the tip–sample configuration on approach and retraction, respectively, for the tip located on top of one of these atoms at a distance of 4.75 Å. At this tip–sample distance the biggest difference in approach/retraction forces occurs. During approach the repulsive force of ≈1 nN, acting in this particular situation, results in the overall displacement of the carbon atoms towards the Ag surface by 0.1 Å and a visible deformation of the tip apex—the Ag atom is moved to the base of the tip—while the tip retracts from the surface. In this case, the dissipation

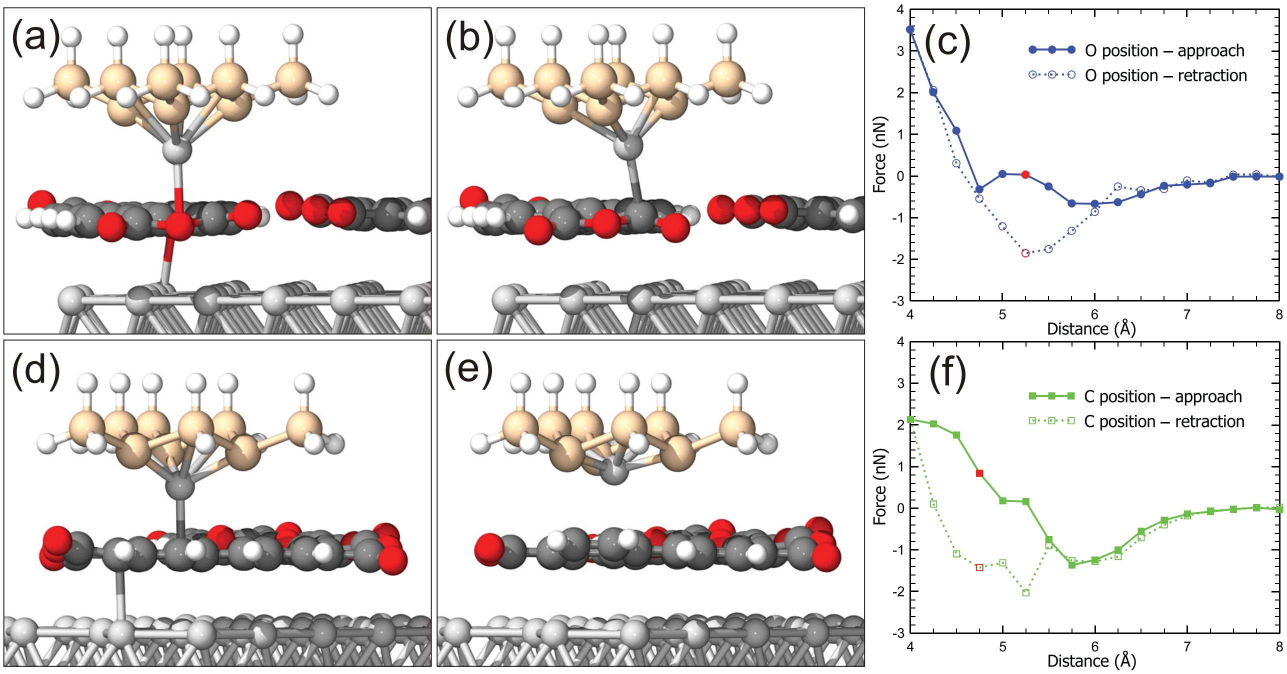

Figure 8. Side views of the tip–sample geometry for the Ag-Si tip approaching on: a) top of the anhydride oxygen atom and d) a carbon atom in the perylene core of the molecule. b,e) Tip–sample geometry during retraction of the Ag-Si tip on the oxygen and carbon positions, respectively. The tip–sample distance is 5.25 Å for (a) and (b) and 4.75 Å for (d) and (e) with respect to the last Ag layer. Color code for the atoms: oxygen (red), silver (light gray), carbon (dark gray), hydrogen (white), and silicon (light salmon). c,f) Force versus distance curves for the approach and retraction of the Ag-Si tip on: c) O position and f) C position. The red symbols correspond to the tip–sample configurations shown in (a,b) and (d,e), respectively.

mechanism is likely to involve two different bonding configurations of the whole molecule during tip approach and retraction, which were not accessible with smaller tip indentations.

The comparison of the absolute energy dissipation values between our DFT simulations for the Ag-Si tip with the experiments is shown in Figure 5. The calculated values (especially the dissipation at the ends) match reasonably well for distances up to 5 Å, which is still in the attractive or near-contact force regime. For the larger indentation, our theoretical results are clearly above the experimental values, although they reproduce correctly the experimental trend that the dissipation signal from the centers of the molecules becomes dominant. We suppose that the inadequacy of our small nanoasperity to describe correctly the elastic response of the tip–sample system could be responsible for these deviations. In general, one has also to consider that the experiments were performed at room temperature while the theory is based on simulations for $T = 0$ K. Therefore, differences in the dissipation between experiment and theory are to be expected as calculations predict smaller force hysteresis and, thus, reduced dissipation with increasing temperature.[56] Furthermore, the smaller contrast in the dissipation between the molecule sites observed in the experiment could result from a relatively blunt tip in contrast to the tip apex considered in the simulations, which ends in a single Ag atom.

The details of the different bonding configurations of the two molecules should affect the energy landscape and thus the dissipation. Our calculations prove that this is indeed the case: molecule A, almost in registry with the surface, behaves differently in the absolute dissipation energies and the distance evolution of the contrast from molecule B (see Figures 5 and 6). Both molecules show the left–right asymmetry between the dissipation at its ends, but molecule B reproduces better the trends found in the experiment. As only one of the molecules of the unit cell was used to produce the average experimental results for dissipation, our results suggest that molecule B is the one considered. However, a conclusive identification would also require a comparison with experimental results obtained for the other orientation within the unit cell.

6. Conclusion

We have compared force and dissipation spectroscopy experiments on a PTCDA monolayer adsorbed on Ag(111) with first-principles calculations based on DFT. From the 3D force spectroscopy measurements, we have extracted force and dissipation curves that can be assigned to different parts of the molecules. Based on the interaction strength observed in the experimental force curves, an Ag-contaminated Si nanoasperity has been identified for the the tip apex. The absolute values of the calculated dissipation for this tip structure, assuming adhesion hysteresis as origin, agree reasonably well with the experimental data. Our experiments reveal systematic differences in the dissipative interactions between the end groups and the center of the molecules that change with the tip–sample distance. DFT calculations provide an explanation for the observed trends in terms of the competition between localized dissipation mechanisms involving the quite mobile oxygen atoms on the sides of the molecule, and global molecular deformations involving the more rigid perylene core. These results confirm adhesion hysteresis as the dominant dissipation mechanism in the near-contact regime and provide a firm basis for the use of dissipation imaging as a tool for achieving intramolecular resolution and for the identification of functional groups in other complex organic systems.

Acknowledgements

Financial support by the Deutsche Forschungsgemeinschaft (DFG) through the transregional collaborative research center TRR 061 (project B7), the Spanish MICINN (projects MAT2008-02929-NAN, MAT2008-02939-E, and CSD2010-00024), the Comunidad de Madrid (project S2009/MAT-146), and the ESF (AFRI project within the FANAS Eurocores Programme), and computer time provided by the Spanish Supercomputing Network (RES) and by the CeSViMa (Madrid) are gratefully acknowledged.

This Full Paper is part of the Special Issue on Multilevel Molecular Assemblies: Structure, Dynamics, and Functions, featuring contributions from the Transregional Collaborative Research Center (TRR 61).

---

[1] F. J. Giessibl, *Science* **1995**, *267*, 68–71.
[2] M. A. Lantz, H. J. Hug, R. Hoffmann, P. J. A. van Schendel, P. Kappenberger, S. Martin, A. Baratoff, H.-J. Guntherodt, *Science* **2001**, *291*, 2580–2583.
[3] H. Hölscher, S. M. Langkat, A. Schwarz, R. Wiesendanger, *Appl. Phys. Lett.* **2002**, *81*, 4428–4430.
[4] A. Schirmeisen, H. Hölscher, U. D. Schwarz, *Noncontact Atomic Force Microscopy II*, Springer-Verlag, Berlin, **2009**, Ch. 5.
[5] C. Seidel, A. Schäfer, H. Fuchs, *Surf. Sci.* **2000**, *459*, 310–322.
[6] T. Yoda, T. Ichii, T. Fukuma, K. Kobayashi, H. Yamada, K. Matsushige, *Jpn. J. Appl. Phys.* **2004**, *43*, 4691–4694.
[7] B. Such, D. Weiner, A. Schirmeisen, H. Fuchs, *Appl. Phys. Lett.* **2006**, *89*, 093104.
[8] L. Gross, F. Mohn, N. Moll, P. Liljeroth, G. Meyer, *Science* **2009**, *325*, 1110–1114.
[9] H. J. Hug, A. Baratoff, *Noncontact Atomic Force Microscopy*, Springer-Verlag, Berlin **2002**, Ch. 20.
[10] S. Morita, R. Wiesendanger, E. Meyer, *Noncontact Atomic Force Microscopy, NanoScience and Technology*, Springer-Verlag, Berlin **2002**.
[11] R. García, R. Pérez, *Surf. Sci. Rep.* **2002**, *47*, 197–301.
[12] F. J. Giessibl, M. Herz, J. Mannhart, *Proc. Natl. Acad. Sci. USA* **2002**, *99*, 12006–12010.
[13] N. Oyabu, P. Pou, Y. Sugimoto, P. Jelínek, M. Abe, S. Morita, R. Pérez, O. Custance, *Phys. Rev. Lett.* **2006**, *96*, 106101.
[14] W. Denk, D. W. Pohl, *Appl. Phys. Lett.* **1991**, *59*, 2171–2173 .
[15] P. Grütter, Y. Liu, P. LeBlanc, U. Dürig, *Appl. Phys. Lett.* **1997**, *71*, 279–281.
[16] C. Loppacher, R. Bennewitz, O. Pfeiffer, M. Guggisberg, M. Bammerlin, S. Schär, V. Barwich, A. Baratoff, E. Meyer, *Phys. Rev. B* **2000**, *62*, 13674–13679.
[17] R. Bennewitz, A. S. Foster, L. N. Kantorovich, M. Bammerlin, C. Loppacher, S. Schär, M. Guggisberg, E. Meyer, A. L. Shluger, *Phys. Rev. B* **2000**, *62*, 2074–2084.
[18] M. Gauthier, R. Pérez, T. Arai, M. Tomitori, M. Tsukada, *Phys. Rev. Lett.* **2002**, *89*, 146104.
[19] A. Schirmeisen, H. Hölscher, *Phys. Rev. B* **2005**, *72*, 045431.
[20] A. Schirmeisen, D. Weiner, H. Fuchs, *Phys. Rev. Lett.* **2006**, *97*, 136101.
[21] V. Caciuc, H. Hölscher, D. Weiner, H. Fuchs, A. Schirmeisen, *Phys. Rev. B* **2008**, *77*, 045411.
[22] S. A. Ghasemi, S. Goedecker, A. Baratoff, T. Lenosky, E. Meyer, H. J. Hug, *Phys. Rev. Lett.* **2008**, *100*, 236106.
[23] B. J. Albers, T. C. Schwendemann, M. Z. Baykara, N. Pilet, M. Liebmann, E. I. Altman, U. D. Schwarz, *Nat. Nanotechnol.* **2009**, *4*, 307–310.
[24] A. Volokitin, B. Persson, *Phys. Rev. B* **2003**, *68*, 155420.
[25] M. Gauthier, M. Tsukada, *Phys. Rev. B* **1999**, *60*, 11716–11722.
[26] N. Sasaki, M. Tsukada, *Jpn. J. Appl. Phys.* **2000**, *39*, L1334–L1337.
[27] L. N. Kantorovich, T. Trevethan, *Phys. Rev. Lett.* **2004**, *93*, 236102.
[28] N. F. Martínez, W. Kamiński, C. J. Gómez, C. Albonetti, F. Biscarini, R. Pérez, R. García, *Nanotechnology* **2009**, *20*, 434021.
[29] W. Kamiński, R. Pérez, *Tribol. Lett.* **2010**, *39*, 295–309.
[30] A. Gerlach, S. Sellner, F. Schreiber, N. Koch, J. Zegenhagen, *Phys. Rev. B* **2007**, *75*, 045401.
[31] F. Tautz, *Prog. Surf. Sci.* **2007**, *82*, 479–520.
[32] S. Duhm, A. Gerlach, I. Salzmann, B. Bröker, R. Johnson, F. Schreiber, N. Koch, *Org. Electron.* **2008**, *9*, 111–118.
[33] S. Picozzi, A. Pecchia, M. Gheorghe, A. Di Carlo, P. Lugli, B. Delley, M. Elstner, *Phys. Rev. B* **2003**, *68*, 195309.
[34] A. Hauschild, K. Karki, B. C. C. Cowie, M. Rohlfing, F. S. Tautz, M. Sokolowski, *Phys. Rev. Lett.* **2005**, *94*, 036106.
[35] R. Rurali, N. Lorente, P. Ordejn, *Phys. Rev. Lett.* **2005**, *95*, 209601.
[36] A. Hauschild, K. Karki, B. C. C. Cowie, M. Rohlfing, F. S. Tautz, M. Sokolowski, *Phys. Rev. Lett.* **2005**, *95*, 209602.
[37] L. Romaner, D. Nabok, P. Puschnig, E. Zojer, C. Ambrosch-Draxl, *New J. Phys.* **2009**, *11*, 053010.
[38] T. R. Albrecht, P. Grütter, D. Horne, D. Rugar, *J. Appl. Phys.* **1991**, *69*, 668–673.
[39] K. Ruschmeier, A. Schirmeisen, R. Hoffmann, *Phys. Rev. Lett.* **2008**, *101*, 156102.
[40] B. Gotsmann, C. Seidel, B. Anczykowski, H. Fuchs, *Phys. Rev. B* **1999**, *60*, 11051–11061.
[41] C. Loppacher, R. Bennewitz, O. Pfeiffer, M. Guggisberg, M. Bammerlin, S. Schär, V. Barwich, A. Baratoff, E. Meyer, *Phys. Rev. B* **2000**, *62*, 13674–13679.
[42] P. Jelínek, H. Wang, J. P. Lewis, O. F. Sankey, J. Ortega, *Phys. Rev. B* **2005**, *71*, 235101–235109.
[43] M. A. Basanta, Y. J. Dappe, P. Jelínek, J. Ortega, *Comput. Mater. Sci.* **2007**, *39*, 759–766.
[44] O. F. Sankey, D. J. Niklewski, *Phys. Rev. B* **1989**, *40*, 3979–3995 .
[45] G. Kresse, J. Furthmüller, *Phys. Rev. B* **1996**, *54*, 11169.
[46] W. Kohn, L. J. Sham, *Phys. Rev.* **1965**, *140*, A1133–A1138.
[47] A. Tkatchenko, L. Romaner, O. T. Hofmann, E. Zojer, C. Ambrosch-Draxl, M. Scheffler, *MRS Bull.* **2010**, *35*, 435–442.
[48] M. Rohlfing, R. Temirov, F. S. Tautz, *Phys. Rev. B* **2007**, *76*, 115421.
[49] A. Kraft, R. Temirov, S. K. M. Henze, S. Soubatch, M. Rohlfing, F. S. Tautz, *Phys. Rev. B* **2006**, *74*, 041402 (R).
[50] Y. Zou, L. Kilian, A. Schöll, T. Schmidt, R. Fink, E. Umbach, *Surf. Sci.* **2006**, *600*, 1240–1251.
[51] P. Pou, S. A. Ghasemi, P. Jelínek, T. Lenosky, S. Goedecker, R. Pérez, *Nanotechnology* **2009**, *26*, 264015.
[52] S. T. Bromley, M. A. Zwijnenburg, T. Maschmeyer, *Phys. Rev. Lett.* **2003**, *90*, 035502.
[53] U. Dürig, *Appl. Phys. Lett.* **1999**, *75*, 433–435.
[54] G. Cross, A. Schirmeisen, A. Stalder, P. Grütter, M. Tschudy, U. Dürig, *Phys. Rev. Lett.* **1998**, *80*, 4685–4688.
[55] G. Langewisch, H. Fuchs, A. Schirmeisen, *Nanotechnology* **2010**, *21*, 345703.
[56] T. Trevethan, L. Kantorovich, *Nanotechnology* **2006**, *17*, 205–212.

Received: September 14, 2011

DOI: 10.1002/smll.201101919